

# A classification of wave generation characteristics during large wave events on the Southern Australian margin

M.A. Hemer<sup>a,\*</sup>, I. Simmonds<sup>b</sup>, K. Keay<sup>b</sup>

<sup>a</sup>*CSIRO Marine and Atmospheric Research, GPO Box 1538, Hobart 7001, Tasmania, Australia*

<sup>b</sup>*School of Earth Sciences, University of Melbourne, Parkville, Vic., Australia*

Received 4 September 2007; received in revised form 5 November 2007; accepted 12 December 2007

Available online 23 December 2007

## Abstract

The Southern Australian continental margin is exposed to some of the largest waves of the global ocean, having been generated by Southern Ocean extra-tropical storms. Waverider buoy data from four buoys which span the full 3000 km length of the Southern Australian continental margin, supplemented with 10 years of numerical model output from the WAVEWATCH III wave model, have been used to describe the directional wave climate of the region. The buoy records include two records at the western end of the margin (a 10-year record from Rottneest Island, and an 8-year record from Cape Naturaliste); a 6-year record from Cape de Couedic in the central portion of the margin; and a record spanning 20 years from Cape Sorell, at the southeastern end of the margin. Cape Sorell exhibits the steepest waves, largest mean significant wave heights, and most westerly wave directions, indicating increased proximity to Southern Ocean wave generating storms. Rottneest exhibits the least steep, smallest mean significant wave heights, and most southerly wave directions, reflecting the greater distance from the Southern Ocean generating storms. All sites demonstrate highly energetic extreme events, particularly at Cape Sorell, and a predominance of swell over wind sea states.

Spatial coherence between simultaneous buoy records show that wave events are easily tracked in the wave record as they propagate eastwards along the Southern Australian margin. Maximum correlation between records indicates that wave events at Cape Sorell lag those at Rottneest by approximately 80 h, and at Cape de Couedic by approximately 7 h. The speed of propagation of events between records is therefore consistent with the propagation speeds of extra-tropical cyclones along the Southern Australian margin.

Synoptic typing of six-hourly mean sea level pressure (MSLP) patterns obtained from the NCEP–NCAR reanalysis has been carried out to determine the main synoptic types associated with large wave events at the Cape Sorell waverider buoy site. Significant differences occur in wave characteristics between synoptic types. At Cape Sorell, wave event magnitude shows a significant correlation to the intensity (as measured by the depth) of the forcing cyclone, with larger wave events occurring during more intense storms in the Southern Ocean. At the other buoy sites, the magnitude of wave events shows little correlation to the intensity of the storm, but is more closely related to the location of the storm, with larger events occurring when storms are closer to the Australian continent. These relationships are of importance for determining how the wave climate might change in this region (and how Australia's coastline might respond) in response to changes in atmospheric forcing which are currently being observed.

© 2007 Elsevier Ltd. All rights reserved.

**Keywords:** Wave climate; Wave statistics; Australia; Extra-tropical cyclone

## 1. Introduction

Knowledge of the wave climate acting on a specific area is important for most coastal engineering and management projects. Design characteristics of coastal or offshore infrastructure are typically dependent on maximum wave

heights, and the sediment budget of a stretch of coastline is dependent on transport processes which depend, in turn, on the magnitude, wavelength and direction of the incoming waves.

The advent of satellite altimeter wave measurements and the use of global wave models have greatly increased our knowledge of waves in the Southern Ocean (e.g., Young, 1999; Alves and Young, 2003). Satellite altimeters, however, are only reliably able to measure significant wave

\*Corresponding author. Tel.: +61 3 62325017.

E-mail address: [mark.hemer@csiro.au](mailto:mark.hemer@csiro.au) (M.A. Hemer).

heights. Gommenginger et al. (2003) present a simple empirical model to estimate wave periods using altimeter data; however, Caires et al. (2005) show this method to be reliable only in regions where waves are locally generated, showing poor comparison to modelled wave periods in swell dominated regions, such as the Southern Australian margin. The global wave models are subject to the uncertainties of all models of environmental processes (discretisation of time and space, propagation of errors in forcing and boundary conditions, etc.). Consequently, Waverider buoys remain the most reliable observations of wave conditions which provide long-term (several years) wave data.

Some of the world's largest surface ocean waves are observed in the Southern Ocean south and southwest of the Australian continent (Sterl and Caires, 2005). Despite this, or perhaps as a result of this, in situ wave observations along the Southern Australian margin of sufficient length to describe the wave climate are scarce. The first Waverider buoys to measure a full annual cycle of waves off the Southern Australian margin were deployed in 1985 off the west coast of Tasmania, at the Cape Sorell site (Fig. 1; Reid and Fandry, 1994), before being recovered in 1992. In the mid-late 1990s, additional Waverider buoys were deployed along the Southern Australian margin offshore of Rottneest Island, and at Cape Naturaliste in Western Australia; at Cape de Couedic, South Australia, and a waverider buoy was redeployed at the Cape Sorell site, west of Tasmania. Together these waverider buoy records allow a spatial network of wave data in the region, which spans more than 20 years.

Other wave data are available along the Southern Australian margin, however is of insufficient length to describe the wave climate of the region. In 1984, Provis and Steedman (1985) deployed a number of wave measuring devices along a cross-continental shelf transect on the eastern side of the Great Australian Bight, South Australia. They measured wave transformations across the

continental shelf for a period of 5 months from mid-May to mid-October of that one year. Reid and Fandry (1994) have described the Cape Sorell wave climate; however, additional data collected since that study enable greater statistical certainty to be determined in the analysis. Reid and Fandry (1994) collected the previously mentioned Cape Sorell wave record, in addition to several other wave records of shorter duration at various sites around Tasmania. The Cape Sorell record is the only record of multiyear length, suitable for describing a wave climate. Hemer and Bye (1999) carried out a modelling study of the swell climate of the South Australian sea, aiming to describe the swell climate, and the dissipation of swell energy as it propagates into Spencer Gulf, and Gulf St. Vincent on the South Australian coast. Lemm et al. (1999) describe the offshore Perth wave climate, using 2.5 years of wave data from the Rottneest waverider buoy. Johnson and Pattiaratchi (2004) gathered intermittent wave data in the Recherche Archipelago, Western Australia, for 3 months in 1 month blocks. They combined these results with a modelling study to describe the wave climate in the Archipelago, aimed at determining the wave driven influence of benthic disturbance in the region. Wood et al. (2005) measured waves south of Australia over a 6-month period from early April 2004, the emphasis of the study being the application of an upward looking ADCP to measure waves. Another notable short wave record which exists in this region are the results of the Southern Ocean Wave Experiment (SOWEX; Banner et al, 1999). All of these studies have commented on the long-period Southern Ocean swell dominating the wave climate; however, the length of each of these studies has been insufficient to adequately describe the Southern Australian wave climate, and the spatial variability of this climate along the 3000 km southern margin of the Australian continent.

It is widely acknowledged that large wave events on the Southern Australian continental margin are a direct response to the passage of extra-tropical cyclones in the

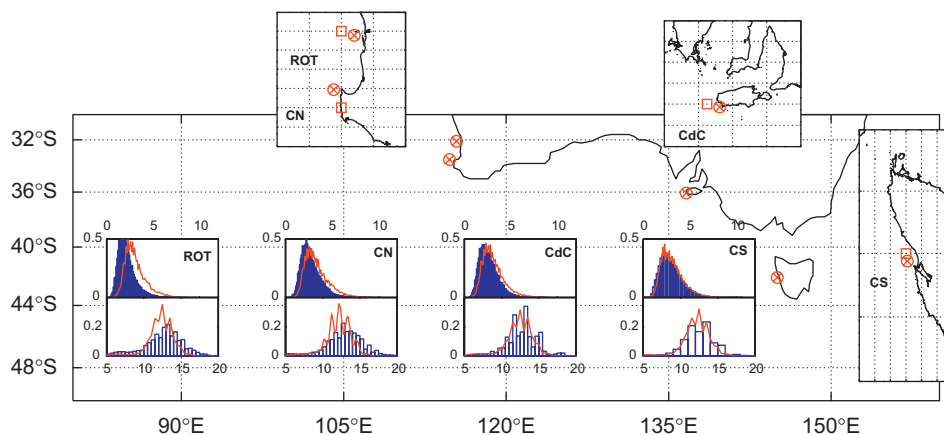


Fig. 1. Location of waverider buoys on the Southern Australian continental margin. Inset maps display local setting for each buoy (CS, Cape Sorell; CdC, Cape de Couedic; CN, Cape Naturaliste; ROT, Rottneest) marked by the cross-circle, and the adjacent WW3 grid point, marked by the open square. Inset distributions display significant wave height (m; upper) and peak wave period (s; lower) distributions for each buoy record (marked as ROT, CN, CdC and CS, respectively). Block distributions indicate buoy data, line distributions indicate WW3 data.

region. The details of this relationship, however, are unstudied. For example, it is not known whether the magnitude of a storm wave event is more closely associated with the magnitude, path, or duration of the forcing extra-tropical storms in the region. The aims of this study are to first determine the nature, sources and variability of waves on the Southern Australian margin, and secondly understand the details of the relationship between wave events and the passage of extra-tropical cyclones along the Southern margin, and determine how the synoptic situation influences the characteristics of a wave event.

This paper is presented in five sections. This introduction is followed by an analysis of the wave climate of the Southern Australian continental margin, describing the available wave data, and the statistical results for significant wave height, peak wave period, wave power (or wave energy flux) and peak wave direction. Analysis of wave steepness, and the extreme wave climate in the region are also presented. Section 3 describes the spatial inter-relationships between the Southern Australian buoy records; Section 4 describes the synoptic situations which lead to generation of wave events at the buoy sites, including the location, nature, characteristics and variability of these systems. The results of the study are summarised in Section 5.

## 2. The wave climate of the Southern Australian continental margin

### 2.1. Available wave data

Data have been obtained from four waverider buoys located on the southern margin of the Australian continent (Fig. 1). Waverider buoy data for this study have been obtained from three sources. The Department of Planning and Infrastructure, Government of Western Australian operates a number of waverider buoys on the Western Australian coast. Data from the Cape Naturaliste and Rottneest buoys have been used for this study. The Australian Government Bureau of Meteorology (BoM) operate two waverider buoys: one located 10 km to the southwest of Cape de Couedic, Kangaroo Island, South

Australia, and the other located 10 km west of Cape Sorell, off the west coast of Tasmania (Fig. 1). Reid and Fandry (1994) deployed a waverider buoy at the Cape Sorell site from 1985 to 1993, and these data are archived at the CSIRO. There was a 5-year gap before the BoM re-deployed the waverider buoy at the same location in 1998. All treatment of the Cape Sorell data in this study combines the CSIRO deployment of the late 1980s–early 1990s with the BoM deployment. The 5-year time gap between records is treated the same as all data gaps greater than 6 h in length. For each of the four buoy records, data have been obtained for the period from buoy deployment through to the end of 2006. Table 1 summarises the buoy records obtained for the study.

In this work, we have focused our analysis on four statistical wave parameters: significant wave height,  $H_S$ ; peak wave period,  $T_P$ ; peak wave direction,  $D_P$ ; and wave energy flux, or deepwater wave power,  $P_O$  calculated using the formula (from Holthuijsen, 2007):

$$P_O = \frac{1}{16} \rho g H_S^2 C_g,$$

where  $\rho$  ( $\text{kg m}^{-3}$ ) is the average density of seawater,  $g$  ( $\text{ms}^{-2}$ ) is the acceleration due to gravity,  $H_S$  is the significant wave height, and  $C_g$  ( $\text{ms}^{-1}$ ) is the wave group velocity. As the waverider buoys are located in 50–100 m water depth, the deepwater wave assumption is not always valid for the long Southern Ocean swell. Consequently,  $C_g$  is determined using the equation  $C_g = n\lambda/T$ , where  $\lambda$  is wavelength determined using a numerical iterative solution (Newton–Raphson method) of the dispersion relationship,  $T$  is taken as the mean wave period, and  $n$  is (Holthuijsen, 2007):

$$n = \frac{1}{2} \left( 1 + \frac{4\pi d/\lambda}{\sinh(4\pi d/\lambda)} \right)$$

which varies from  $n = 1/2$  for deep water, and  $n = 1$  for very shallow water,  $d$  is water depth.

Of the buoy records, directional data are available only from the Rottneest buoy for the last 15 months of the record (September 2005–December 2006). Wave direction is an important parameter to the determination of longshore sediment transport along such wave-dominated coast, and

Table 1  
Overview of wave datasets used

Location	Latitude (°S)	Longitude (°E)	Water depth (m)	Dates	Data source
Cape Sorell (CS)	42.15	145.02	100	11 July 1985, 24 September 1992	CSIRO
	42.12	145.03	100	23 March 1998, 31 December 2006	BoM
Cape de Couedic (CdC)	36.07	136.62	80	1 November 2000, 31 December 2006	BoM
Cape Naturaliste (CN)	33.36–33.52	114.78–114.76	50	7 November 1998, 31 December 2006	WADPI
Rottneest (ROT)	32.11	115.40	50	25 July 1991, 31 December 2006	WADPI
CS—WW3	42	145	100	1 February 1997, 31 December 2006	WW3
CdC—WW3	36	136	150	1 February 1997, 31 December 2006	WW3
CN—WW3	34	115	100	1 February 1997, 31 December 2006	WW3
ROT—WW3	32	115	1250	1 February 1997, 31 December 2006	WW3

the directional wave climate for this region has not been previously described. To study the directional wave climate, wave data were obtained from the National Centers for Environmental Prediction (NCEP) online archive (website <http://polar.ncep.noaa.gov/waves/>). This data archive contains numerical output from the third generation spectral wave model WAVEWATCH III (Tolman et al., 2002; Tolman, 2002) developed at NCEP. The characteristics of this dataset, hereafter referred to as WW3, which spans the period from the beginning of 1997 through to the end of 2006 are summarised in Table 1. Data from WW3 grid cells adjacent to each buoy site were used to describe the directional wave climate at each location, and the locations of the centre of these grid cells are plotted in Fig. 1.

To counteract the variable temporal resolution of the waverider buoy records, wave data were re-sampled at hourly intervals. Data gaps of greater than 6 h were maintained as data gaps (i.e., filled with NaN's), and gaps shorter than 6 h were linearly interpolated.

## 2.2. Statistical results

The probability distribution of  $H_S$  and  $T_P$  from waverider buoy data at each location is plotted in Fig. 1. The variance of  $H_S$  is greatest at Cape Sorell (S.D.: 1.19 m), indicating that largest wave heights are observed at this location. Rottneest indicates the smallest median wave height at 1.99 m. The variance of wave periods is greatest at Cape Naturaliste and Rottneest (S.D.: 2.56 and 2.79 s, respectively). Cape Sorell and Cape de Couedic are typically closer to the generating storms, and therefore swell periods observed at these locations are not as long as at the Western Australian sites.

Monthly mean  $H_S$ ,  $T_P$  and  $P_O$  from each waverider buoy record were determined, and the means of the monthly means are plotted in Fig. 2 to illustrate the seasonal cycle of wave height, period and power in the data. A strong seasonal cycle of  $H_S$ ,  $T_P$  and  $P_O$  is evident at all locations, with larger waves of longer period and greater power observed during the winter months.

### 2.2.1. Significant wave height

Mean monthly  $H_S$  are typically greater at Cape Sorell than other buoy sites throughout the year (Fig. 2a). The phase of the annual cycle of  $H_S$  differs between buoy sites, varying between a spring (September) peak at Cape Sorell, and a winter (July) peak at Cape Naturaliste. Strongest seasonal variability is apparent at Cape Naturaliste (S.D.: 0.513 m). Comparisons with Cape de Couedic (which exhibits annual mean  $H_S$  of similar magnitude; 2.70 and 2.63 m, respectively) indicate that summer mean  $H_S$  are greater at Cape de Couedic, yet winter mean  $H_S$  are greater at Cape Naturaliste. The smallest seasonal variability of the four sites occurs at Cape Sorell (S.D.: 0.332 m), with relatively steady large  $H_S$  throughout the year. The

annual cycle of  $H_S$  at Rottneest is consistent with that described by Lemm et al. (1999) using the shorter record.

Interannual variability within each month is typically greatest at all sites during winter months, indicating the large variability in winter storms. However, peak inter-annual variability at Cape Naturaliste is observed in November, indicating large spring variability.

### 2.2.2. Peak wave period

Peak wave periods show little variability between sites (Fig. 2b). Monthly mean peak wave periods are greater than 10 s throughout the year at all sites. Table 2 shows that at all sites, peak wave periods are almost always greater than 8 s, indicating that the long period, Southern Ocean swell dominates the wave signal at all four of the southern margin sites.

Wave periods are longer during the winter months (April–September), during which period monthly mean  $T_P$  at Cape Sorell is approximately 1 s shorter than at the other sites. The increased proximity of the Cape Sorell site to the Southern Ocean storms is the likely factor. Only during December have monthly mean peak wave periods been shorter than 10 s, and only at Rottneest and Cape Naturaliste (Rottneest in years 1995 and 2001, Cape Naturaliste in year 2001). Longest monthly mean wave periods are observed at Cape Naturaliste, with the peak of the annual cycle occurring during July, with mean peak period of 13.76 s. The peak of the annual cycle at Cape Sorell is observed in September, with periods of 13.12 s.

### 2.2.3. Wave energy flux

The importance of the wave period, or wavelength, to the wave power calculation is apparent when comparing the wave power at the four sites. Despite wave height being greatest at Cape Sorell, we see that the largest wave power is observed at Cape Naturaliste during July, when long-period waves of large magnitude are observed (Fig. 2c). Largest monthly wave power values are observed at Cape Sorell for all months except June, July, August and November, during which Cape Naturaliste has the greatest magnitude wave energy fluxes. During summer months, Cape de Couedic wave energy flux values are greater than those at Cape Naturaliste, illustrating the strong annual cycle at Cape Naturaliste with respect to Cape de Couedic (S.D. of annual cycle of  $2.2e4$  and  $1.3e4 \text{ W m}^{-1}$ , respectively). The integrated wave power throughout the year is greatest at the Cape Sorell site.

### 2.2.4. Directional wave climate

The second stage of the analysis combined the buoy data and the WW3 data. Firstly, confidence in the WW3 directional data needs to be established. Directional data are available from the Rottneest buoy for a full 12 months during the year 2006. Fig. 3 displays the probability density plot of peak direction  $D_P$  as a function of the significant wave height  $H_S$  using Rottneest buoy data (sea and swell states, separated by partitioning the wave spectra wave

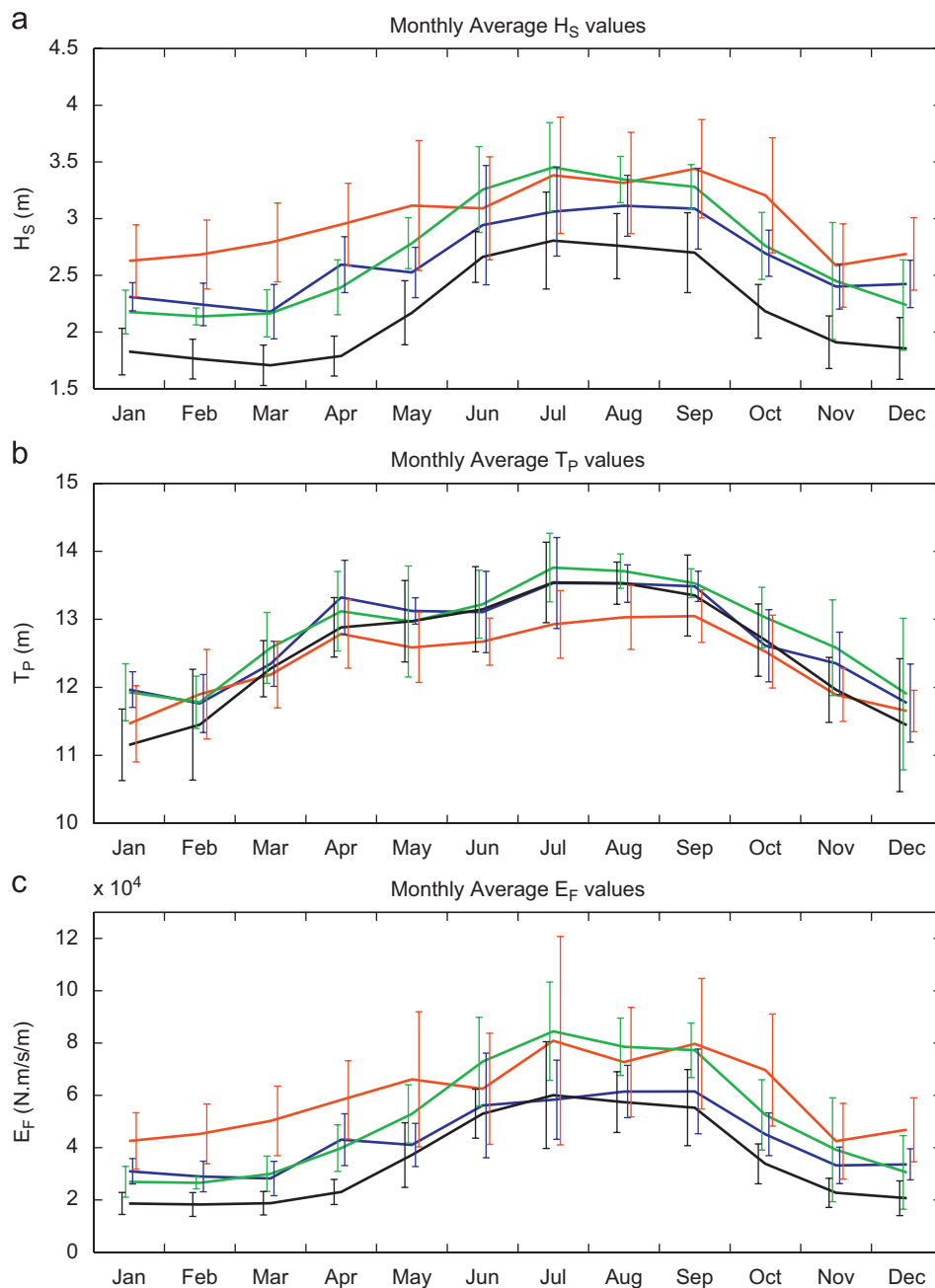


Fig. 2. Mean annual cycle of (a) significant wave height (m); (b) peak wave period (s) and (c) wave power (or wave energy flux,  $\text{N}\cdot\text{m}/\text{s}/\text{m}$  wave crest), from the Southern Australian margin waverider buoys. Solid lines represent mean annual cycle at ROT (black), CN (green), CdC (blue) and CS (red). Monthly interannual variability of each variable is displayed by standard deviation bars of the same colour on each record.

Table 2  
Percentage of peak wave period data that exceeds 8 s

Location	Percentage of data, $T_p > 8$ s
CS	97.6
CdC	96.8
CN	95.2
ROT	91.9

period 8 s) and 2006 ROT-WW3 data, respectively (WW3 spectral data are not available from the Rottneest site, and can therefore not be separated into sea and swell states).

The density plot shows the WW3 significant wave height is greater than the buoy measured swell and sea wave heights, and the WW3 directional data to have a greater southerly component than the buoy measured sea or swell direction, with an approximate  $20^\circ$  difference between peak wave directions. A portion of the wave direction difference may be explained by wave refraction with propagation towards the coast. The WW3 grid point lies offshore of the buoy (in water depth of over 1000 m). The buoy lies in nearshore waters of water depth of 50 m. The WW3 data indicate waves propagate towards the coast at an angle of approximately  $45^\circ$  normal to the coastline (assuming

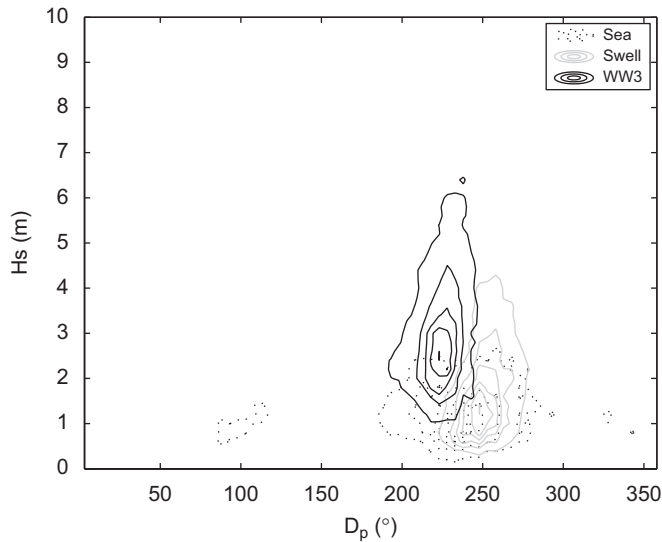


Fig. 3. Density plot of  $D_P$  versus  $H_S$  comparing WW3 directional data and waverider buoy directional data at Rottneest for the year 2006. WW3 data (black contours); buoy sea state (dotted contours); buoy swell state (gray contours). The buoy is situated in approximately 50 m water depth; the adjacent WW3 grid point is in approximately 1200 m water depth. Contour lines are plotted for values: 0.001%, 0.005%, 0.01%, 0.015%, 0.02%, 0.03%, 0.04% and 0.05%.

northsouth aligned depth contours). Swell waves, as they approach the coast, will refract to propagate more perpendicular to the coast (i.e., a greater westerly component), as is observed by the buoy. The amount of expected wave refraction can be easily determined using the Snells law relation ( $\sin \phi/c = \text{constant}$ , where  $\phi$  is the direction of waves with respect to the normal of the depth contours, and  $c$  is the wave phase speed). A 12.5 s wave (mean  $T_P$  at Rottneest; Fig. 2b) will refract about  $10^\circ$  between 1200 and 50 m water depths. Thus, there is potentially a  $10^\circ$  directional bias between buoy and WW3 directional data, with WW3 waves having a greater southerly component than buoy measured direction.

In the buoy measured sea wave component, a secondary sea state with waves directed from the east is observed. These are waves experienced during offshore winds, and are not expected to have a large impact on the coast.

Fig. 4 displays the probability plot of peak direction  $D_P$  as a function of the significant wave height  $H_S$  using wave height data from the buoy records, and peak direction data from the WW3 data. Wave data were interpolated onto times at which wave height data are available from the hourly buoy record. Directional distributions at Cape Naturaliste and Rottneest are very similar, with most wave events, particularly the most energetic events ( $H_S > 3$  m), having a directional spread of  $220\text{--}240^\circ\text{N}$ , centred at approximately  $225^\circ\text{N}$ . At Cape Sorell, the large wave events have a greater directional spread, with waves greater than 3 m significant wave height having a spread from  $220^\circ\text{N}$  to  $260^\circ\text{N}$ , centred at approximately  $235^\circ\text{N}$ . The directional climate at Cape de Couedic is slightly more southerly than Cape Sorell, with directions being centred

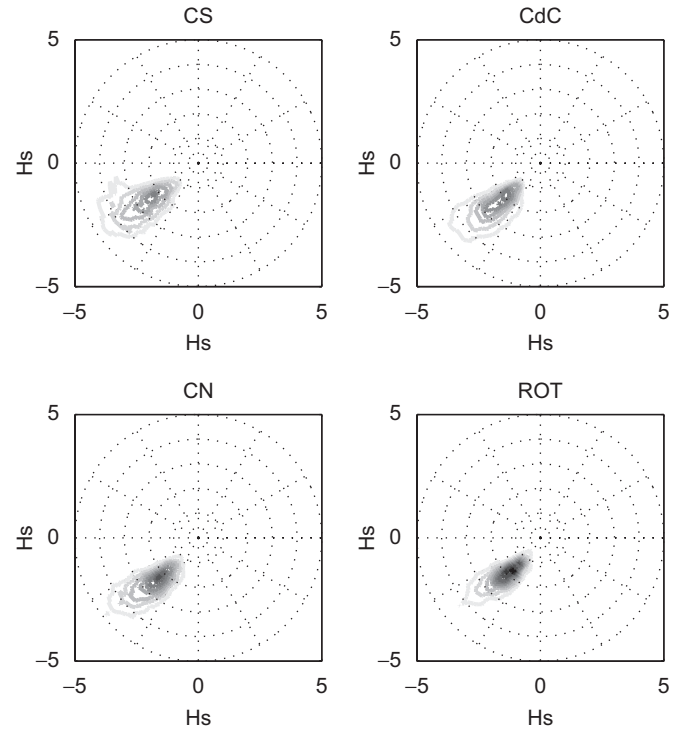


Fig. 4. Density rose plots of peak wave direction versus  $H_S$  at Cape Sorell (CS; top-left); Cape de Couedic (CdC; top-right); Cape Naturaliste (CN; lower-left) and Rottneest (ROT; lower-right). Wave directions are taken from WW3 data; at times  $H_S$  data are available from buoy records. Radial distance of plots corresponds to  $H_S$  in units of metres. Angle corresponds to wave approach direction. Contour lines are plotted for values: 0.001%, 0.005%, 0.01%, 0.015%, 0.02%, 0.03%, 0.04% and 0.05%.

at approximately  $230^\circ\text{N}$ , and spreading from  $210^\circ\text{N}$  to  $240^\circ\text{N}$ .

Seasonal directional variability of wave events is subtle, given almost all waves originate from the southwest quadrant. To determine the characteristics of the directional variability, the southwest quadrant is split into five segments bounded by  $180^\circ\text{N}$ ,  $205^\circ\text{N}$ ,  $220^\circ\text{N}$ ,  $230^\circ\text{N}$ ,  $245^\circ\text{N}$  and  $270^\circ\text{N}$ . Fig. 5 shows the frequency distribution of  $H_S$  in each directional segment for data from Cape de Couedic (which displays consistent patterns to all other sites). Largest wave heights occur in the more westerly wave segments:  $230\text{--}245^\circ\text{N}$  and  $245\text{--}270^\circ\text{N}$ . The most westerly waves ( $245\text{--}270^\circ\text{N}$ ) occur predominantly during the winter months (May–October), and have a broad spectrum of wave heights ( $H_S$  averaging 3.3 m, with seasonal means less than 3 m during summer and autumn only). Similarly, southerly waves ( $D_P < 220^\circ\text{N}$ ) occur predominantly during the summer and autumn (DJF and MAM) and have smaller wave heights ( $H_S$  averaging 2.55 m, with no seasonal means exceeding 3 m). Waves occurring from  $220^\circ\text{N}$  to  $245^\circ\text{N}$  occur year round, with  $H_S$  averaging less than 3 m throughout the year, but wave periods are greatest from these directional segments (mean 12.8 and 13.2 s from the  $220^\circ\text{N}$  to  $230^\circ\text{N}$  and  $230^\circ\text{N}$  to  $245^\circ\text{N}$  segments, respectively). Data from the whole southwest quadrant (Fig. 5F) indicate winter patterns

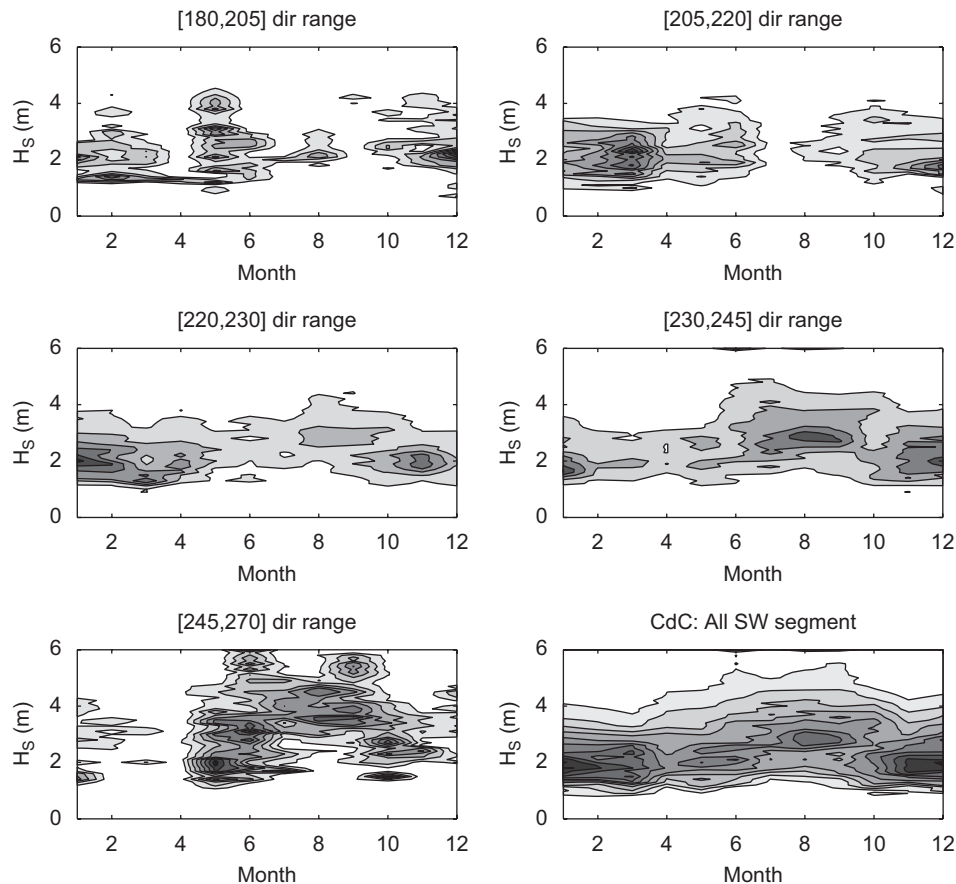


Fig. 5. Directional frequency distribution of wave height  $H_S$  at Cape de Couedic, showing the monthly occurrence (in days per month) of waves from given directional sectors: 180–205°N (top-left); 205–220°N (top-right); 220–230°N (mid-left); 230–245°N (mid-right); 245–270°N (lower-left); and 180–270°N (lower-right).

(May–September) are dominated by a broader spectrum of wave heights (and wave periods, not shown), and summer patterns have a less broad distribution of wave height (and period) occurrence.

### 2.3. Wave steepness

Fig. 6 displays the density plot relating peak periods and significant wave heights at each buoy site. A curve relating to the maximum steepness ( $H/\lambda$ ) of a fully developed sea in deep water (1/19.7) according to Pierson–Moskowitz (PM) relationships (Pierson and Moskowitz, 1964) has been added to each subplot. The curve of constant steepness, which defines the centre of the normalised histogram, has also been added.

Two groups are distinguished in each of the subplots. One group centres on short peak wave periods of between 5 and 7 s, and wave heights of approximately 2 m. This group is more pronounced at the Cape Naturaliste and Rottneest buoy sites. At Cape Sorell, this short period group is almost indistinguishable. This group lies only slightly to the right of the PM steepness curve and therefore constitutes intermediate sea states between wind seas and swell. The second group centres on long peak wave periods of 10–15 s, of similar energy levels (centred on wave heights

of approximately 2 m). This group constitutes most of the sample at all locations, and is composed only of swell events of low steepness values. Peak period typically increases with wave height in both groups. The second curve, which indicates the centre of the histogram illustrates differences in wave conditions between the four sites. The steepness is greatest at Cape Sorell, followed by Cape Naturaliste, Cape de Couedic, and is least at Rottneest, suggesting Cape Sorell and Cape Naturaliste are closer to regions of wave generation. By the time that waves reach Rottneest and Cape de Couedic, wave energy has dissipated and the steepness of the observed swell is less than that observed in a region of generation.

### 2.4. Extreme value statistics

Extreme value statistical analysis can be employed for studying extreme weather and climate variability in a broad range of disciplines. Available wave buoy  $H_S$  data have been analysed using extreme value statistics to relate the behaviour of the extreme events to the mean and standard deviation of the wave height. The magnitude of extreme wave events are usefully described by their return period (the average time between events of a particular height) and

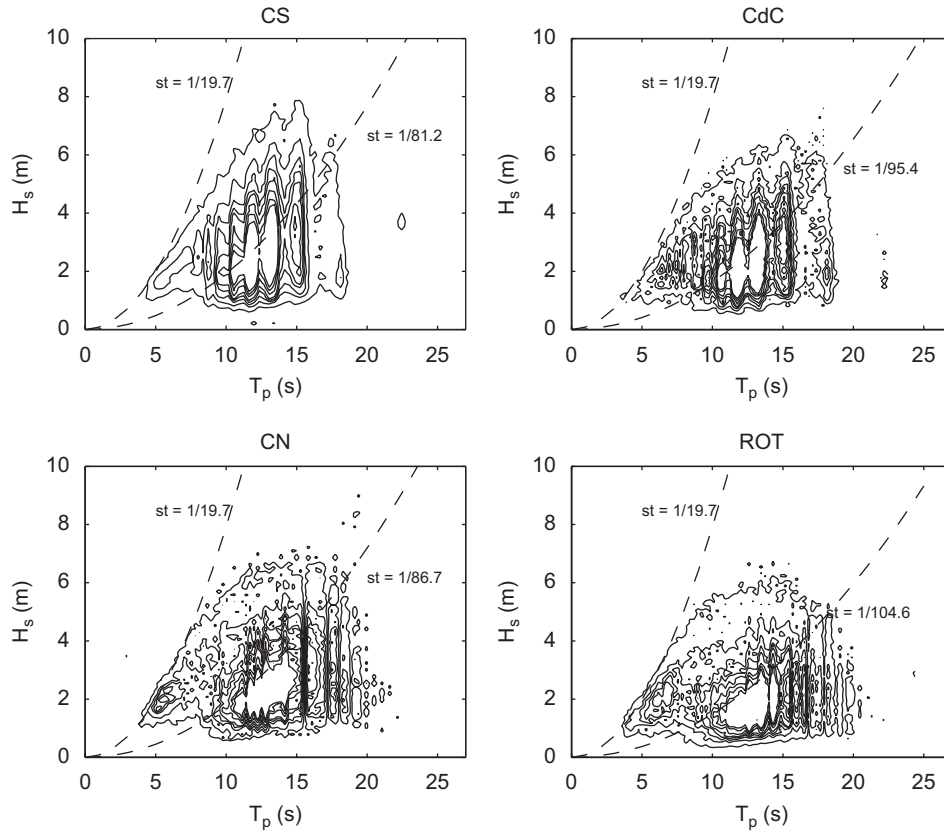


Fig. 6. Density plot of  $T_p$  versus  $H_S$  for the four buoy records: Cape Sorell (top-left); Cape de Couedic (top-right); Cape Naturaliste (lower-left) and Rottneest (lower-right). Dashed lines are drawn for lines of constant steepness. Contour lines are plotted for values: 0.001%, 0.005%, 0.01%, 0.015%, 0.02%, 0.03%, 0.04% and 0.05%.

their return period value (the wave heights of events given a return period, i.e., a 100-year storm event).

Following Ferreira and Guedes-Soares (1998), the return period value estimates have been determined using the peaks-over-threshold (POT) method (Coles, 2001). The POT method consists of fitting the Generalised Pareto distribution (GPD) to the peaks of clustered excesses over a threshold,  $u$ . The excesses over a threshold  $u$  of a time-series  $X_1, X_2, X_3 \dots$  are the observations (called exceedances)  $X_i - u$  such that  $X_i > u$ . A peak excess is defined as the largest excess in a cluster of exceedances. In this paper, a cluster is defined as a group of consecutive exceedances. However, clusters have been further reduced in number by merging clusters where the threshold upcrossing is less than 2 days after the threshold downcrossing of the previous event—having assumed that these clusters are likely to be in response to the same event. By fitting the distribution to the peak excesses, independence is ensured.

In the POT method, the peak excesses are assumed to occur according to a Poisson process with rate  $\lambda_u$ , and to be independently distributed with a GPD, given by

$$F_u(x) = \begin{cases} 1 - \left(1 - \frac{\kappa x}{\alpha}\right)^{1/\kappa}, & \kappa \neq 0 \\ 1 - \exp\left(-\frac{x}{\alpha}\right), & \kappa = 0 \end{cases}$$

where  $\kappa$  and  $\alpha$  are shape and scale parameters, respectively, and  $x$  is in the range  $(0, \infty)$  if  $\kappa \leq 0$  and  $(0, \alpha/\kappa)$  for  $\kappa > 0$ .

Two qualitative graphical approaches have been used to select a threshold. First, the GPD has been fit to the peak excesses using a range of thresholds. The shape and scale parameters have been graphed as a function of the chosen threshold, and an appropriate threshold chosen as the lowest threshold such that any higher threshold chosen would result in similar estimates. Second, an important property of the GPD is that if  $\kappa > -1$ , then the mean exceedance over a threshold  $u$  is a linear function of the threshold  $u$ . Consequently, the mean threshold exceedance was plotted as a function of  $u$ , and the lower limit of linearity was chosen as a suitable threshold. For each dataset, the two methods provided a consistent estimate of the threshold.

Once the threshold was chosen, and the peak excesses extracted from the time-series, the scale ( $\alpha$ ) and shape ( $\kappa$ ) parameters of the GPD were estimated using the maximum likelihood method (e.g., Hosking and Wallis, 1987). The yearly cluster rate,  $\lambda_u$  was estimated by the average number of clusters/peak excesses per year. The buoy data used in this study contain several gaps. Consequently,  $\lambda_u$  is calculated according to the amount of available data, not the time span of the record. For example, if 20 events are recorded over a 2-year time period, but the record has a

3-month data gap,  $\lambda_u$  is calculated as 11.4 events per year, as opposed to 10 events per year if the record was assumed to be 2 years long. This simpler method was chosen in preference to filling in gaps with WW3 data, or adjacent buoy data adjusted for time lags and regression corrections.

If the number of peak excesses per year is a Poisson random variable with mean  $\lambda_u$ , the expected number of peak excesses in  $N$  years is  $N\lambda_u$ . If the peak excesses over  $u$  are independently distributed with distribution function  $F_u$ , then the expected number of observations exceeding  $x$  is  $N\lambda_u (1 - F_u(x))$ . Setting this equal to 1, and solving for  $x$  gives  $x_N^u$ , the  $N$ -year return period value for a threshold  $u$ , given by

$$x_N^u = \begin{cases} u + \left(\frac{x}{\kappa}\right)(1 - (\lambda_u N) - \kappa), & \kappa \neq 0 \\ \alpha \log(\lambda_u N), & \kappa = 0 \end{cases}$$

Confidence intervals for the return period value estimates have been determined using the profile likelihood approach.

Chosen thresholds, the number of peak exceedances, the mean yearly cluster rate, the maximum likelihood fitted parameter values and return period values for  $N = 1, 5, 10$  and 100 are given for each wave record in Table 3. The extreme wave statistics derived using the POT method indicate relatively large annual return wave heights at all stations (well in excess of the mean wave height at each station). The ratio between centennial to annual wave heights provides some insight into the type of weather systems which force wave events at the site. If the centennial wave height is of similar magnitude to the annual wave height, this indicates that the wave climate is relatively steady. A large increase between annual return wave height and centennial wave height indicates the buoy is prone to rare, very large events. However, such a ratio is also dependent on the length of record, and how many large rare events are counted in the statistics. Therefore, comparisons can only be made using records of the same length. Here, this is most easily done comparing the statistics obtained from the four WW3 points, each being determined from a 10-year time-series. The largest increase is observed at the Cape Naturaliste site, which displays 31% increase from annual return  $H_5$  to centennial return  $H_S$ . Cape Sorell and Rottneest both display a 24% increase and Cape de Couedic increases by 22%.

Best estimate 1- and 100-year peak  $H_5$  values at Rottneest, determined by Lemm et al. (1999) using the Weibull method, of 6.7 and 9.8 m, respectively, compare well to the corresponding values of 6.87 and 9.57 m determined in this study, despite the short record used by Lemm et al. Similarly, previous estimates of the 100-year return period value at the Cape Sorell buoy site have been determined by fitting the three Fisher-Tippett (Gumbel, Frechet and Weibull) distributions to all events greater than 6 m in the first 6.1 years of the Cape Sorell waverider buoy record (i.e., the CSIRO deployment; Reid and

Table 3  
Extreme wave statistics for given wave records using the peaks over threshold method

Record	$u$ (m)	$M$	$\lambda_u$	$\alpha$	$\kappa$	Negative log-likelihood	$X_1^u$	$X_5^u$	$X_{10}^u$	$X_{100}^u$
CS (15.0)	6.7	97	6.5	1.145 (0.145)	0.065 (0.077)	104.1	8.71 (8.37, 9.14)	10.26 (9.67, 11.37)	10.88 (10.17, 12.46)	12.75 (11.50, 15.10)
CS—CSIRO (6.1)	6.7	29	4.77	1.004 (0.271)	-0.108 (0.197)	32.3	8.41 (7.84, 9.35)	10.50 (9.25, 13.52)	11.52 (9.84, 15.35)	15.51 (11.55, 22.51)
CS—BoM (8.9)	6.7	69	7.74	1.328 (0.202)	0.270 (0.099)	70.3	8.79 (8.44, 9.20)	9.78 (9.37, 10.69)	10.10 (9.65, 11.34)	10.80 (10.19, 12.63)
CS—WW3 (10)	6.7	59	5.9	1.060 (0.186)	0.233 (0.121)	48.7	8.24 (7.83, 8.60)	9.18 (8.52, 10.07)	9.49 (8.75, 10.77)	10.22 (9.29, 12.04)
CS—CERA40 (44.2)	6.7	193	4.37	1.177 (0.113)	0.257 (0.067)	174.8	8.14 (7.98, 8.33)	9.21 (8.98, 9.53)	9.54 (9.29, 9.99)	10.32 (9.92, 11.34)
CdC (6.1)	5.5	74	12.2	0.835 (0.124)	0.173 (0.095)	47.8	7.19 (6.91, 7.59)	7.95 (7.57, 8.92)	8.22 (7.78, 9.41)	8.91 (8.25, 10.40)
CdC—WW3 (10)	5.5	137	13.7	1.251 (0.151)	0.256 (0.088)	132.6	7.89 (7.62, 8.24)	8.73 (8.37, 9.55)	9.00 (8.58, 10.09)	9.61 (8.97, 11.07)
CN (7.7)	5.8	80	10.4	1.288 (0.191)	0.321 (0.104)	74.5	7.92 (7.65, 8.29)	8.68 (8.31, 9.51)	8.91 (8.59, 10.01)	9.38 (9.02, 10.95)
CN—WW3 (10)	5.8	144	14.4	1.218 (0.143)	-0.156 (0.084)	150.0	8.46 (8.13, 8.92)	9.60 (9.10, 10.77)	10.01 (9.40, 11.47)	11.10 (10.07, 12.93)
ROT (13)	4.8	161	12.4	0.925 (0.107)	0.096 (0.084)	132.9	6.87 (6.61, 7.22)	7.95 (7.49, 8.91)	8.37 (7.79, 9.57)	9.57 (8.46, 11.18)
ROT—WW3 (10)	5.3	143	14.3	1.292 (0.131)	0.238 (0.061)	145.5	7.85 (7.56, 8.19)	8.76 (8.41, 9.44)	9.06 (8.67, 9.93)	9.76 (9.23, 11.09)

Columns of the table are wave record (number of years of record in years in brackets); chosen threshold ( $u$ ); number of events ( $M$ ); cluster rate ( $\lambda$ ); maximum likelihood estimates of the scale ( $\alpha$ ) and shape ( $\kappa$ ) parameters (and their standard error in brackets); the negative log likelihood value; return period values ( $X$ ) for 1-, 5-, 10- and 100-year return periods (95% confidence intervals in brackets, determined using profile likelihood method), which are a function of the chosen threshold,  $u$ .

Fandry, 1994). The 100-year return period values determined using these three distributions are 14.62, 17.42 and 12.4 m, respectively. Using the POT extreme statistics on the same dataset, the 100-year return period value is 15.51 m, with 95% confidence intervals of 11.55–22.51, displaying no significant difference to previous estimates. However, the Cape Sorell return period values are very sensitive to the length of record used. The return period values are sensitive to the 13.2 m event which occurred in July 1985. We find that if statistics are derived from only the CSIRO Cape Sorell record, the shape parameter  $\kappa$  is less than zero (although standard error contains zero and positive values), suggesting a heavier (decreases more slowly) type II tail, as opposed to all other fitted distributions which display lighter, type III tails. Statistics derived using only the later BoM Cape Sorell wave record significantly underestimates the previous return period values. Using both records combined, the fitted distribution has smaller errors, and a narrower band of confidence, indicating the importance of longer records when deriving extreme values.

Previous comparisons of extreme sea states between buoy data and WW3 data have indicated the WW3 data resulted in more extreme sea states (Abadie et al., 2006). This was interpreted as offshore extreme wave states being more energetic than those nearer to shore. Although WW3 statistics are not determined from the same length record as the buoy statistics, WW3 return period values overestimate the buoy derived values at all sites except Cape Sorell, which comes about due to the influence of the large July 1985 wave event which occurred before the WW3 record commenced. Comparing only the later BoM Cape Sorell record and the WW3 derived values, we see that the WW3 estimates are slightly larger than those from the buoy record. Similar to Abadie et al. (2006), the WW3 record at all sites is taken from a site deeper than the buoy record. No conclusions can be made as to whether offshore wave statistics are more energetic than those nearshore, or that WW3 statistics are more energetic than the buoy derived values.

### 3. Inter-relationship between wave records

Waves arrive at each of the southern margin buoys from the southwest quadrant throughout the year, with periods of 7–20 s and significant wave heights up to 12 m. In this section, we establish the inter-relationships between wave records to determine whether wave events observed at each location are also observed at the other locations, and if so, whether the primary relationship is a response to relatively stationary distant storms with waves propagating to all sites, or a response to storms propagating along the southern margin.

Four waverider buoys results in six pairs of buoys to compare (CS–CdC, CS–CN, CS–ROT, CdC–CN, CdC–ROT, CN–ROT). Twelve data pairs, consisting of hourly time-series, were prepared (six  $H_S$ , six  $T_P$ ). Missing

data in a record were removed from the other paired record. For each data pair, a correlation analysis was carried out to determine the maximum correlation, and the time lag (up to a maximum 108 (4.5) h (days)) at which the maximum correlation occurred. This time lag is interpreted as the average period of time that it takes a wave event to travel from the first site (western most) to the second site (eastern most). Fig. 7 displays the correlations vs time lag between paired  $H_S$  records and paired  $T_P$  records.

Correlation between data records is typically greater for  $H_S$  than  $T_P$  (Table 4). However, the time lag which yields maximum correlation using  $T_P$  as the key variable is approximately half the time lag which leads to maximum correlation if  $H_S$  is the key variable, for all station pairs (Table 4).

A time lag of 30–60 h (~2 days) is observed between an event being observed at Cape Naturaliste and being observed at Cape Sorell. This speed of propagation is similar to the speed of synoptic scale storms (extra-tropical cyclones) which propagate along the southern margin of the Australian continent, suggesting events are primarily associated with propagating storms, as opposed to distant storms creating a large swell which propagates towards all sites simultaneously.

### 4. Wave generation along the Southern Australian margin

The climate along the Southern Australian margin is dominated by the passage of extra-tropical cyclones and associated frontal systems which propagate from west to east south of the Australian continent, with a period of approximately 6–8 days (Simmonds and Keay, 2000a). The seasonal shift of the northern most margin of the Southern Ocean storm belt from approximately 45°S during the summer months, northwards to approximately 35°S during winter (Hurrell et al., 1998) leads to seasonal variability of the wave climate as observed in the previous sections. This section aims to describe the dominant pressure systems which lead to large wave events along the Southern Australian margin, describing their nature and location and how this is expressed in the observed wave climate.

Wave records were assessed for only the period for which data were available from all four buoy records (i.e., November 2000–December 2006). A database of wave events was compiled for each buoy record. Wave events were defined as those periods when  $H_S$  exceeded the mean  $H_S$  plus two standard deviations. A clustering procedure was then carried out to merge wave events which occurred close together in time (events were considered close together if the time between a threshold upcrossing and the previous threshold downcrossing was less than 2 days). Similarly, events which consisted of only one value above the threshold were removed from the events database.

Events at each site were classified as being observed only at that location, at a pair of locations, at a set of three locations, or at all locations. Based on the results of the previous section, a maximum time difference of 4 days was

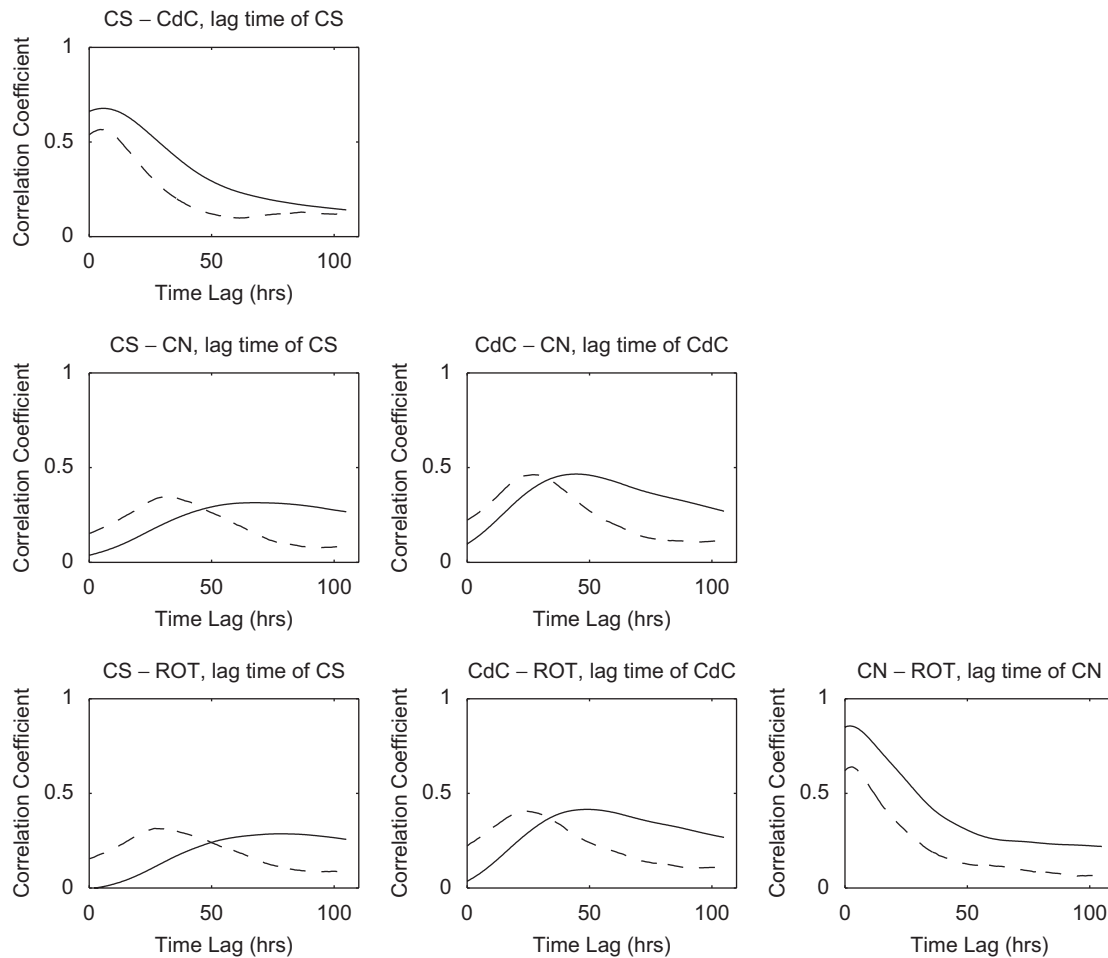


Fig. 7. Correlation analysis of wave height  $H_S$  (solid line) and peak wave period ( $T_P$ ) records, showing time lag (in hours) versus Pearson correlation coefficient for record pairs: (upper-left) CS–CdC; (mid-left) CS–CN; (mid) CdC–CN; (lower-left) CS–ROT; (bottom-middle) CdC–ROT and (lower-right) CN–ROT.

Table 4  
Correlation and time lags between site pairs using  $H_S$  and  $T_P$  as key variables

Site pair	$H_S R_{\max}$	$H_S T_{\text{lag}}$ (hours)	$T_P R_{\max}$	$T_P T_{\text{lag}}$	Distance between sites (km)	Speed (m/s)
CS–CdC	0.68	5.8	0.57	4.7	988.9	47–58
CS–CN	0.31	66.6	0.35	32.1	2822.5	12–24
CS–ROT	0.29	77.5	0.31	27.0	2851.2	10–30
CdC–CN	0.47	44.7	0.46	27.2	2014.0	13–20
CdC–ROT	0.42	49.1	0.41	24.2	2001.5	11–23
CN–ROT	0.85	2.1	0.64	2.8	169.0	17–22

specified to separate wave events between sites (e.g., if a wave event at Cape Sorell occurred less than 4 days after that at the other sites, it was deemed to be the same event observed). Table 5 indicates the distribution of events which are observed at single locations or at groups of sites, with respect to the Cape Sorell buoy record.

Less than one half of the wave events observed at Cape Sorell are observed at Cape Sorell only. A large portion of events (37%) are observed at Cape de Couedic as well as Cape Sorell, and 18% of events observed at Cape Sorell, are also observed as large wave events at Cape Naturaliste, and/or Rottneest.

Table 5  
Distribution of events observed at Cape Sorell, indicating number of events which are also observed at other sites

Event observed at	% of CS events
CS only	45
CS and CdC	37
CS, CdC, and CN/ROT	18

Given the proximity of the Rottneest and Cape Naturaliste sites, 85% of the events observed at Cape Naturaliste were also observed at Rottneest. The Rottneest record has

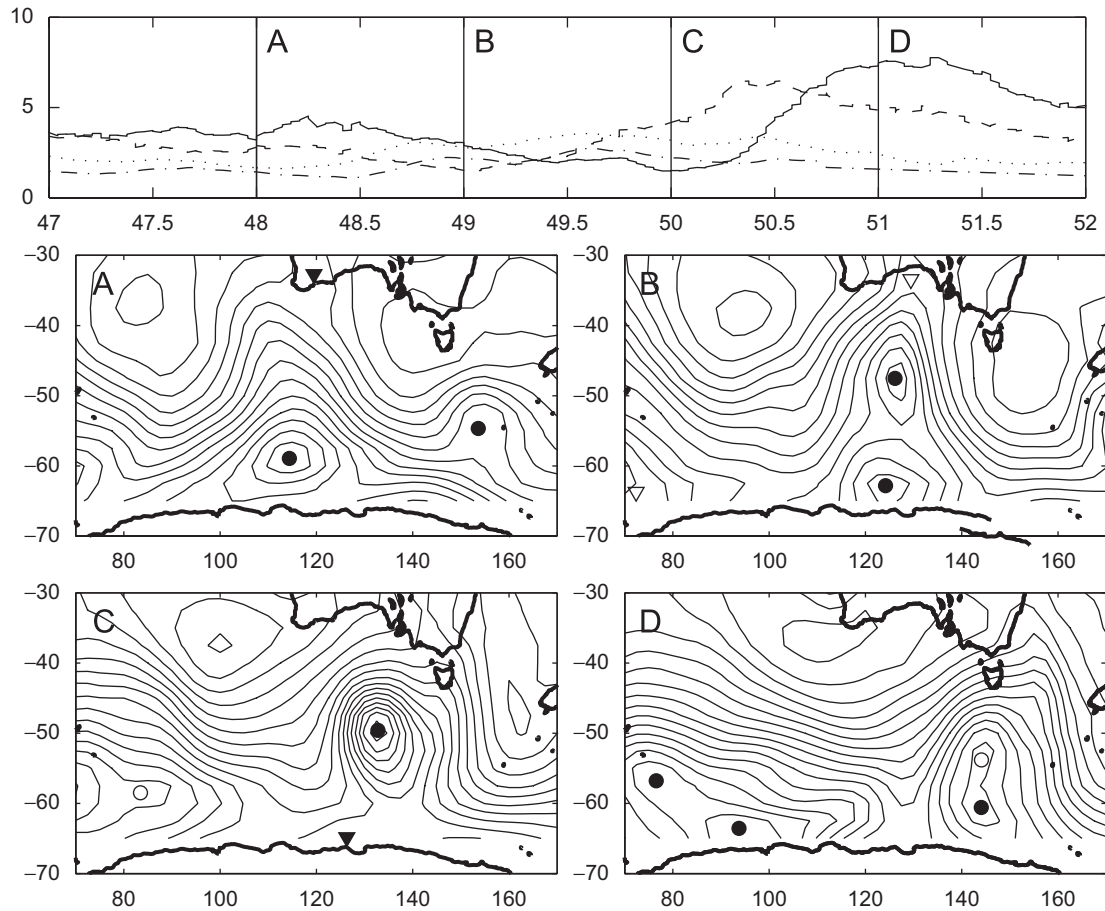


Fig. 8. Storm wave event on the Southern Australian continental margin, February 2002. Upper plot is time-series (day of year, 1992) of significant wave height (m) at four buoy sites (dash dot, Rottneest; dotted, Cape Naturaliste; dashed, Cape de Couedic; solid, Cape Sorell). Subplots (A–D) indicate NCEP–NCAR re-analysis mean sea-level pressure maps at times indicated in upper plot. Contours are at 4 hPa intervals over a range of 940–1030 hPa. Circles indicate centre of extra-tropical cyclone. Solid indicates strong system, open indicates a less strong system, as determined from the Laplacian (Murray and Simmonds, 1991).

therefore been omitted, so that only three records are considered (Cape Sorell, Cape de Couedic and Cape Naturaliste). Focussing on the Cape Sorell record, three categories of event are defined: (i) events observed at Cape Sorell only; (ii) events observed at Cape Sorell and Cape de Couedic; (iii) events observed at Cape Sorell, Cape de Couedic and Cape Naturaliste.

For each event observed at Cape Sorell, the mean sea level pressure (MSLP) record for the 4-days leading up to the event for the region 65–30°S, 70–170°E have been obtained from the NCEP–NCAR atmospheric re-analysis (Kalnay et al., 1996).

NCEP–NCAR MSLP data are provided on a 2.5° geographic grid at six-hourly intervals. The location, radius and depth of mid-latitude cyclones have been identified in these data using the method described by Simmonds et al. (2003). To illustrate the relationship between the synoptic maps and the wave record, Fig. 8 displays the MSLP record for the 4-day period leading up to an event at Cape Sorell which was observed on 21 February 2002. Prior to the event being observed at Cape

Naturaliste and Rottneest, the cyclone can be observed in the Southern Ocean at approximately 60°S, 110°E. An associated cold front was analysed on BoM charts (not shown) extending northwards to the southern margin of the Australian continent. A slight increase in wave height occurs at the western buoys a short time after the passage of the front (these are not classed as events in the database). The event is observed at Cape de Couedic shortly after the same front passes along the South Australia coast, and low pressure system is observed to have shifted further north (50°S, 135°E) and intensified, leading to increased onshore winds towards the Cape de Couedic buoy. As this cyclone propagates eastwards, and travels south of Tasmania, the event is observed at Cape Sorell when the pressure gradient leading to onshore winds to the west coast of Tasmania is greatest. We notice two things from this example: first, that the wave events observed at all sites are in direct response to the front that is associated with the synoptic cyclone which is propagating along the southern margin of the continent (as opposed to a distant swell event), and second, the events observed at

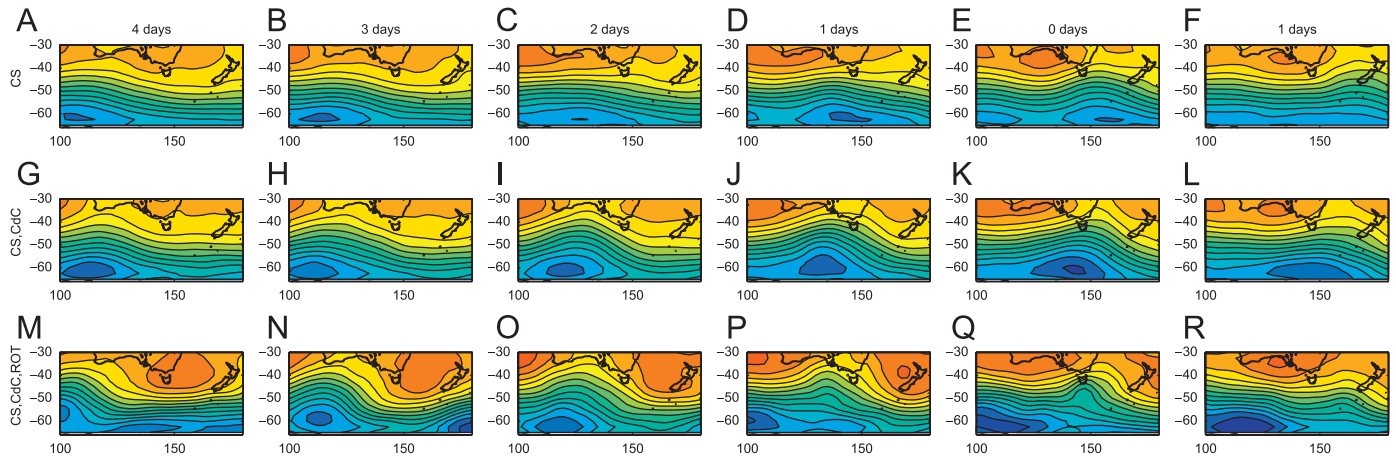


Fig. 9. Composite mean MSLP, for 5 days leading up to categorised Cape Sorell storm wave events. Contours displayed at 4 hPa intervals. Events observed at Cape Sorell only are represented by (A–F), events observed at CS and CdC are represented by (G–L), and events observed at CS, CdC and CN are represented by (M–R). Each row of figures represents a 5-day progression of MSLP charts.

Cape de Couedic and Cape Sorell are much greater than the magnitude of the increase in  $H_S$  observed at Cape Naturaliste and Rottneest, and these coincide with periods when the cyclone is further northwards, nearer to the Southern Australian margin.

Differences in the propagation of synoptic events along the Southern Australian margin must be responsible for whether the wave events can be tracked between the southern buoys. Therefore, two questions arise. First, how do the extra-tropical cyclone propagation tracks differ between wave events which are observed at all buoys, to those where the wave events are observed at only one buoy? Second, is the magnitude of a wave event observed at the buoy a property of extra-tropical cyclone position, and/or depth, where by depth, we refer to that quantity defined in Simmonds et al. (1999) which represents the overall influence of a cyclone including its intensity and scale? We aim to address these questions in this section.

For each category of wave event observed at Cape Sorell (CS only, CS and CdC, or CS, CdC and CN), a composite average of the synoptic situation was determined for the 4 days leading up to the Cape Sorell event. If the wave event is observed in all three southern margin buoys, the low pressure system develops south west of Australia, and propagates across the southern margin (Fig. 9). If the wave event is observed at Cape de Couedic and Cape Sorell only, the cyclone is observed to generate somewhere south of the Australian continent and propagate eastwards from that point (Fig. 9). For wave events which are observed at Cape Sorell only, the cyclone is observed to generate further eastwards again, or shift northwards considerably in this far east region (Fig. 9).

The relationship between wave height at each buoy location, and the position of the centre of a forcing cyclone, is determined by plotting the position of the extra-tropical cyclone as a function of wave height. Mapped grids of significant wave height taken from each buoy location as a function of cyclone location are shown in Fig. 10.

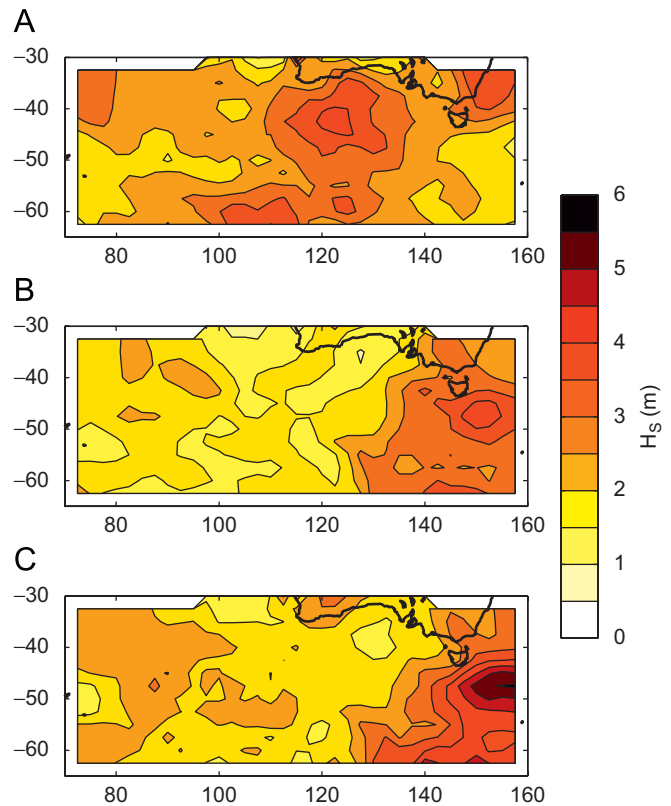


Fig. 10. Storm centre location plotted as a function of significant wave height at locations (A) Rottneest; (B) Cape de Couedic and (C) Cape Sorell.

Maximum wave heights occur at Cape Naturaliste when the centre of the cyclone is located at approximately 40°S, 125°E; at Cape de Couedic when the cyclone is located at approximately 47°S, 150°E; and at Cape Sorell when the cyclone is located at approximately 48°S, 160°E. Maximum wave heights are observed at the buoy sites when the centre of the forcing cyclone is located to the southeast of the buoy, consistent with onshore wind forcing at the buoy site. The depth of cyclones is typically greater further

Table 6  
Correlation between wave height and distance to storm, and wave height and depth of cyclone

	Location	All storms	Closed	Open
Distance	CN	<b>-0.49</b>	<b>-0.45</b>	<b>-0.52</b>
	CdC	<b>-0.46</b>	<b>-0.21</b>	<b>-0.36</b>
	CS	<b>-0.20</b>	-0.06	<b>-0.50</b>
Depth	CN	-0.17	-0.07	<b>-0.263</b>
	CdC	<b>0.27</b>	<b>0.27</b>	0.15
	CS	<b>0.27</b>	<b>0.27</b>	0.07

Bold indicates significance at 95% level.

southwards (Simmonds and Keay, 2000a), yet wave heights are at a maximum when cyclone position is proximal to the waverider buoys. To test this further, the distance of the forcing cyclone centre from the waverider buoy and the depth of the system (using the definition of Murray and Simmonds, 1991) at the time of the peak wave height of an event, is correlated to the peak wave height of the events. This has been carried out for all storms together, for open cyclones, and for closed cyclones (Table 6).

Table 6 indicates that distance to storm is a greater influence on wave height at CN and CdC, however at CS, the magnitude of the correlation between wave height and the depth of the cyclone is greater, suggesting the intensity of the systems is important. The peak wave height of events at Cape Sorell is strongly correlated to the distance from open depressions. The greater proximity of the Cape Sorell buoy site to the Southern Ocean cyclone systems may explain the greater correlation with depth than that with distance, in comparison to the other sites. Another interesting point is that the correlation of wave height and storm distance is greater for the open depressions than it is for the closed depressions, indicating the importance of tracking open systems in the Southern Ocean, where these systems are frequently associated with large heat transports and wild weather.

#### 4.1. Characterising the synoptic situation which lead to large wave events at Cape Sorell

The analyses presented in the previous sections have aimed at characterising the synoptic situation which leads to large wave events along the Southern Australian margin. In this section, an objective classification of the synoptic conditions which occur during large wave events along the Southern Australian margin is carried out. There are several methodologies for formulating synoptic type categories including both subjective and objective procedures (Yarnal, 1993). Objective synoptic typing procedures determine statistically similar and significant synoptic groupings to describe local environmental variables.

Wave events have been identified in the combined Cape Sorell wave record (which spans the period 1985–2006, utilising both the CSIRO and BoM data archives) using the

same method as described in the previous section. The MSLP field at the nearest time after each threshold upcrossing has been obtained from the NCEP–NCAR re-analysis dataset.

An amended Kirchhofer sums-of-squares technique (Kirchhofer, 1973; Yarnal, 1993) which considers points raised by Blair (1998) is used to categorise the synoptic weather maps which lead to large wave events at Cape Sorell. This procedure compares sets of gridded MSLP maps to determine key synoptic maps which force an environmental response (in this case, wave events at Cape Sorell). The results of the analysis are used to relate the atmospheric circulation over the Southern Ocean to large wave events along the Southern Australian margin. To apply the Kirchhofer technique, the MSLP grids are first normalised using:

$$Z_{i,n} = \frac{(x_{i,n} - \bar{x}_n)}{s_n}$$

where  $Z_{i,n}$  is the normalised value of grid point  $i$ , at time  $n$ ,  $x_{i,n}$  is the MSLP at grid point  $i$ ,  $\bar{x}_n$  is the mean of the grid at time  $n$ , and  $s_n$  is the standard deviation of the grid at time  $n$ .

Each normalised grid is compared to other grids using the sums-of-squares equation:

$$S = \sum_{i=1}^N (Z_{i,a} - Z_{i,b})^2$$

where  $S$  is the Kirchhofer score,  $Z_{i,a}$  is the normalised grid value of point  $i$  at time  $a$ ,  $Z_{i,b}$  is the normalised grid value of point  $i$  at time  $b$ , and  $N$  is the number of data points in the grid.

It is possible that a comparison of two grids could generate a low value of  $S$ , indicating overall statistical similarity, but have very different patterns in certain sectors of the synoptic chart. Consequently, to ensure pattern similarity in all parts of the grids, subscore values for each row and column of the grids are also determined.

Grids are considered similar if  $S < N$ ,  $S_R < 1.8N_R$  and  $S_C < 1.8N_C$ , where  $S_R$  and  $S_C$  are the row and column scores, respectively, and  $N_R$  and  $N_C$  are the number of rows and columns in the MSLP grids, respectively.

Scores  $S$ ,  $S_R$  and  $S_C$  are determined for every pair of grids (and rows and columns of) in the sample. If the threshold requirements are met, the pair of grids is considered similar and the  $S$  value is stored. The grid with the most  $S$  values associated with it is designated keygrid 1. That keygrid is stored, along with the number of grids paired to that keygrid, before all the grids which were paired with that keygrid removed. This process repeats to determine subsequent keygrids until all grids are classified into  $m$  groups of five grids or more. Remaining grids are termed ‘unclassified’.

Finally,  $S$ ,  $S_R$  and  $S_C$  are calculated again, this time for each of the original normalised grids with each of the  $m$  keygrids. The lowest Kirchhofer score is recorded for each grid, with the associated keygrid denoting the synoptic type

of that time. Grids can be paired with more than one keygrid, and days misclassified by early removal during the keygrid determination procedure described above, are then reclassified. Once classification has been carried out, all consequent analysis is carried out on the MSLP synoptic maps associated with the normalised keygrids. For each class,  $2 \times m$  maps result: the keygrid (or the original synoptic map for that class, to which most other grids were paired), and the composite mean of MSLP grids for that class. The number of grids which fall into each class are also available. Thus, for every wave event, a synoptic type is prescribed.

Fig. 11 shows the first 10 synoptic types (keygrids) derived from the synoptic typing analysis, which describe 87% of the large wave events at Cape Sorell (Table 7). It is observed that all synoptic types which lead to large wave events at the Cape Sorell waverider buoy display a trough south–southeast of the Australian continent, and a southwesterly airstream directed towards the buoy site. A centre of high pressure is generally observed over the Australian continent, or Great Australian Bight. The location of the centre of anticyclone is critical to the direction of the geostrophic surface winds on the west coast of Tasmania. For example, synoptic type 4 which is the only type which

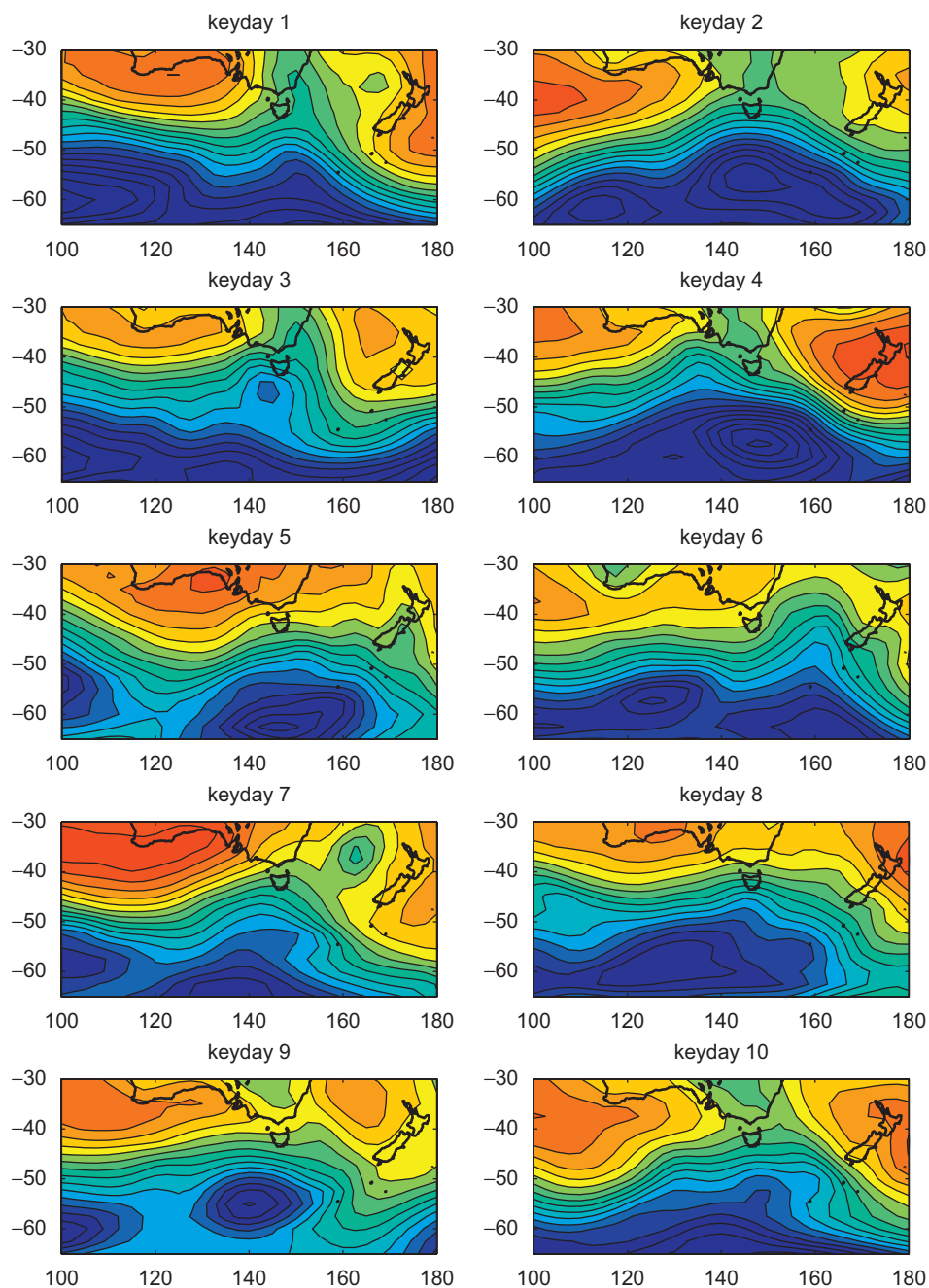


Fig. 11. Key MSLP charts for 10 dominant synoptic types which are found to force storm wave events at Cape Sorell.

Table 7  
Percentage of synoptic maps described by key synoptic types displayed in Fig. 11

Synoptic type	Percentage	Synoptic type	Percentage
1	15.4	6	6.7
2	15.0	7	6.7
3	10.3	8	5.9
4	8.3	9	5.5
5	7.9	10	4.7

does not exhibit a centre of high pressure over the Australian continent is the only type displaying an airstream which has a northerly component. The other type which has a non-distinct centre of high pressure, type 8, displays a due westerly airstream. Fig. 11 indicates that the keygrid for these synoptic types shows the forcing trough is west of Tasmania at the time of the event; and therefore, wave events are probably a response to strong northwesterly winds in the region.

For each wave event, the peak significant wave height, the peak wave period, and the mean peak wave direction have been determined. It is observed that events with the largest wave heights are experienced during synoptic types 8, 7, 9 then 5 (Fig. 12A). An analysis of variance (ANOVA) was carried out to determine whether there is significant difference between the peak significant wave heights experienced from each synoptic type. The ANOVA yields an  $F$ -value of 2.225, ( $p = 0.02172$ ), indicating that there is significant difference in  $H_S$  values between synoptic types at the 95% confidence level. These synoptic types typically display a longer fetch over which winds are blowing than other synoptic types (Fig. 11). As the strong winds blow over these long fetches, the waves grow and propagate towards the Tasmanian west coast, and are observed as the largest of wave events at the Cape Sorell buoy.

The wave period experienced during events displays very little variability between synoptic types, with the mean peak wave period experienced amongst events of all synoptic types being approximately 13.5 s (Fig. 12C). An ANOVA indicates no significant difference of wave periods experienced during events between synoptic types.

Significant differences are observed between wave directions experienced in response to each synoptic type (Fig. 12B). An ANOVA yields an  $F$ -value of 3.115 ( $p = 0.0019$ ) indicating significance at the 99% level. More westerly wave events are experienced during synoptic types 4, 8 and 9. These types describe approximately 20% of the wave events at Cape Sorell. More southerly wave events are experienced during synoptic types 6 and 10, which describe 11.5% of the wave events. Other synoptic types (e.g., type 2) have large ranges of wave directions.

## 5. Summary

This study set the objective of understanding the nature, source and variability of surface ocean waves on the

southern margin of the Australian continent. It is well recognised that this section of coastline is exposed to some of the most energetic waves in the global ocean; however, it is only now that an in situ data record of sufficient length has become available to adequately describe the wave climate of the region.

Significant wave heights are greatest at the southern (and eastern) most buoy site, Cape Sorell on the west coast of Tasmania. This buoy is the only buoy of the four records used which lies south of 40°S, the region commonly described as the “Roaring 40’s”. The increased proximity of Cape Sorell to the Southern Ocean storms appears to be responsible for the larger wave heights observed at this site, relative to the other locations. The peak of the Cape Sorell annual wave height cycle does not occur until September; after the Austral winter months of June, July and August. The phase of the Cape Sorell annual cycle is matched at Cape de Couedic; however, the two western buoys (Cape Naturaliste and Rottneest) have an annual wave height cycle which peaks in the height of winter (July). The Cape Naturaliste June and July mean  $H_S$  values exceeding the Cape Sorell  $H_S$  values, the only periods when the Cape Sorell wave heights are exceeded. During these winter months, wave energy flux (or wave power) has a maximum value of all stations at Cape Naturaliste, displaying the influence of the longer wave periods observed at this site in comparison to the wave periods observed at Cape Sorell. Wave periods are relatively spatially uniform between Cape Naturaliste, Rottneest and Cape de Couedic; however, wave periods are shortest at Cape Sorell of all stations, possibly due to increased proximity to the zone of wave generation.

Differences in wave climate between the sites are interpreted in relation to the position of the site relative to the region waves are generated which arrive at those sites. Mean wave steepness observed at each location indicates steeper waves occur at Cape Sorell and Cape Naturaliste than Cape de Couedic and Rottneest, suggesting these sites are closer to the region of generation.

Wave direction at all four sites is predominantly from the southwest quadrant. However, there are slight differences between sites from which inferences about the location of the generating storms might be made. Wave direction at Cape Sorell has a greater westerly component than the other sites, whereas wave direction at the western sites (Cape Naturaliste and Rottneest) has a greater southerly component. Extra-tropical cyclones propagate approximately westeast, south of the Australian continent. The position of these cyclones tends to force the westerly waves at Cape Sorell, and a greater southerly component the more northwards the buoy is located. Seasonally, the northward shift of the position of extra-tropical cyclones during the winter months drives a shift in wave direction, to have a greater westerly component during this period, and a greater southerly component during summer.

The peaks over threshold extremes analysis method was applied to the  $H_S$  record from each waverider buoy, and also from adjacent WW3 data points. The extreme wave

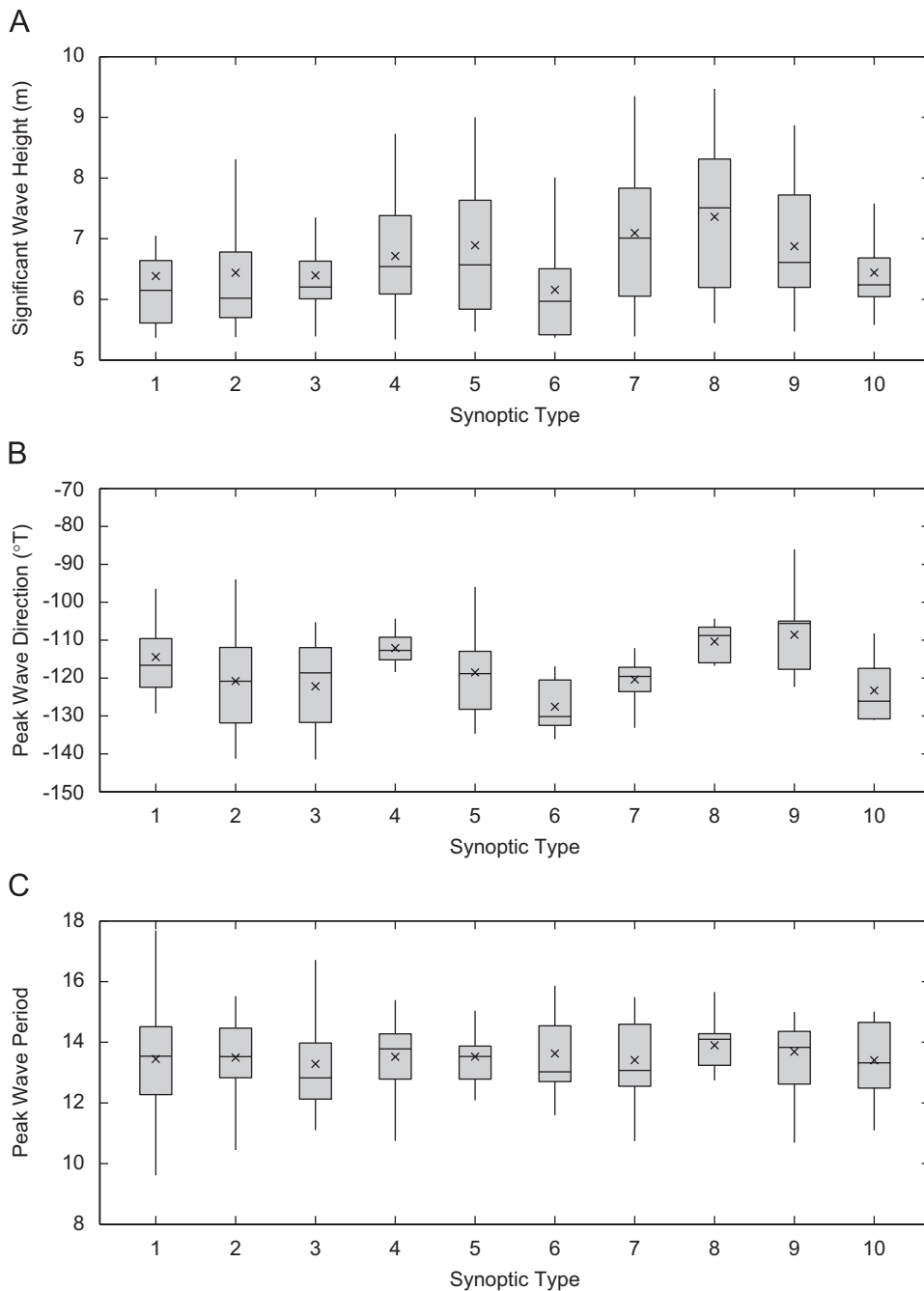


Fig. 12. Boxplots of (A)  $H_S$ , (B)  $D_P$  and (C)  $T_P$  of storm wave event data within each synoptic type.  $H_S$  and  $D_P$  show significant differences between types.

climate is particularly energetic at Cape Sorell, with an annual return  $H_S$  value of 8.71 m. Rottneest displays the least energetic extreme wave climate with annual return  $H_S$  values of 6.87 m. This suggests a latitudinal variation of the extreme wave climate, with increasing energy south, in this region which was evident in the extreme wave statistics presented from the ERA-40 waves re-analysis (Caires and Sterl, 2005).

A large percentage (~20%) of wave events at Cape Sorell can be tracked from the western buoys (Cape Naturaliste) across the Southern Australian margin,

via Cape de Couedic. Maximum correlation between the Cape Naturaliste and Cape Sorell wave height records occur after a time-lag of approximately 3 days, or roughly the time it takes for an extra-tropical storm to propagate along the Southern Australian margin. Wave events which cannot be tracked between buoy records are shown to be forced by synoptic situations where the forcing system has generated south of the Australian continent, or has moved northwards in this region.

Using a synoptic typing procedure, we have presented 10 key synoptic types which lead to large wave events at Cape

Sorell. Significant differences in wave characteristics are observed between different synoptic types, with wave characteristics being sensitive to the position and intensity of forcing weather systems. The magnitude of wave events at all sites appears to be dependent on the position of the forcing system, with larger wave events associated with systems which are centred closer to the buoy. However, the Cape Sorell wave record suggests a stronger relationship with intensity of forcing extra-tropical cyclones in the Southern Ocean south of Australia, than to the distance between system centre and the buoy. Recent trends in the Southern Annular Mode have led to a southern intensification of the Southern Ocean storm belt (Marshall, 2003), where over the past few decades the number of Southern Ocean systems has been decreasing, but their mean intensity increasing (Simmonds and Keay, 2000b). This change in synoptic forcing is likely to lead to changes in the wave climate along the Southern Australian continental margin. Results from this study imply that wave events are likely to increase in magnitude at Cape Sorell, given intensification of the storms, and possibly have a greater southerly component as the centre of these storms shift southwards. This directional shift may also be observed in wave events at those locations slightly further north on the Australian mainland. However, the magnitude of events at these locations may decrease due to the sites susceptibility to the distance from the storm as the centre of storms move southwards away from the Australian coast. Further research to determine how the wave climate in the region (and the consequent Australian coastline) might respond to observed changes in atmospheric forcing is required.

### Acknowledgements

This paper is a contribution to the CSIRO Climate Change Research Program, and is funded with assistance from the Australian Greenhouse Office Climate Change Research Program. The authors acknowledge the suppliers of data: the BoM for the waverider buoy records from Cape Sorell and Cape de Couedic and the Department of Planning and Infrastructure, Government of Western Australia for the waverider buoy records from Cape Naturaliste and Rottnest. MSLP maps were obtained from NCEP–NCAR re-analysis project at NOAA. We also thank Dr. Mike Pook, Dr. Kathy McInnes (CSIRO Marine and Atmospheric Research) and two anonymous reviewers for their reviews of earlier versions of this manuscript.

### References

Abadie, S., Butel, R., Mauriet, S., Morichon, D., Dupuis, H., 2006. Wave climate and longshore drift on the South Aquitaine coast. *Continental Shelf Research* 26, 1924–1939.

Alves, J.H.G.M., Young, I.R., 2003. On estimating extreme wave heights using combined Geosat, TOPEX/Poseidon and ERS-1 altimeter data. *Applied Ocean Research* 25 (4), 167–186.

Banner, M.L., Chen, W., Walsh, E.J., Jensen, J.B., Lee, S., Fandry, C., 1999. The Southern Ocean waves experiment, Part 1: Overview and mean results. *Journal of Physical Oceanography* 29, 2130–2145.

Blair, D., 1998. The Kirchhofer technique of synoptic typing revisited. *International Journal of Climatology* 18, 1625–1635.

Caires, S., Sterl, A., 2005. 100-year return value estimates for ocean wind speed and significant wave height from the ERA-40 data. *Journal of Climate* 18, 1032–1048.

Caires, S., Sterl, A., Gommenginger, C.P., 2005. Global ocean mean wave period data: validation and description. *Journal of Geophysical Research* 110, C02003.

Coles, S., 2001. *An Introduction to Statistical Modelling of Extreme Values*. Springer, London, 228pp.

Ferreira, J.A., Guedes-Soares, C., 1998. An application of the peaks over threshold method to predict extremes of significant wave height. *Journal of Offshore Mechanics and Arctic Engineering* 120, 165–176.

Gommenginger, C.P., Srokosz, M.A., Challenor, P.G., Cotton, P.D., 2003. Measuring ocean wave period with satellite altimeters: a simple empirical model. *Geophysical Research Letters* 30 (22), 2150.

Hemer, M.A., Bye, J.A.T., 1999. The swell climate of the South Australian Sea. *Transactions of the Royal Society of South Australia* 123, 107–113.

Holthuijsen, L.H., 2007. *Waves in Oceanic and Coastal Waters*. Cambridge University Press, Cambridge, UK, 387pp.

Hosking, J.R.M., Wallis, J.R., 1987. Parameter and quantile estimation for the generalized Pareto distribution. *Technometrics* 29, 339–349.

Hurrell, J.W., Van Loon, H., Shea, D.J., 1998. The mean state of the troposphere. *Meteorology of the Southern Hemisphere*. *Meteorological Monographs*, vol. 49. American Meteorological Society, pp. 1–46.

Johnson, D., Pattiaratchi, C., 2004. Prediction and measurement of wave energy and bottom shear stress for Esperance Bay. Centre for Water Research Report No. WP 2051 DJ., Perth, Australia, 36pp.

Kalnay, E., Kanamitsu, M., Kistler, R., Collins, W., Deaven, D., Gandin, L., Iredell, M., Saha, S., White, G., Woollen, J., Zhu, Y., Leetmaa, A., Reynolds, B., Chelliah, M., Ebisuzaki, W., Higgins, W., Janowiak, J., Mo, K.C., Ropelewski, C., Wang, J., Jenne, R., Joseph, D., 1996. The NCEP/NCAR 40-year reanalysis project. *Bulletin of the American Meteorological Society* 77 (3), 437–471.

Kirchhofer, W., 1973. Classification of European 500-mb patterns. *Arbeitsbericht der Schweizerischen Meteorologischen Zentralanstalt Nr. 43*, Geneva.

Lemm, A.J., Hegge, B.J., Masselink, G., 1999. Offshore wave climate, Perth (Western Australia), 1994–96. *Marine and Freshwater Research* 50, 95–102.

Marshall, G.J., 2003. Trends in the Southern Annular Mode from observations and reanalyses. *Journal of Climate* 16 (24), 4134–4143.

Murray, R.J., Simmonds, I., 1991. A numerical scheme for tracking cyclone centres from digital data. Part I: Development and operation of the scheme. *Australian Meteorological Magazine* 39, 155–166.

Pierson Jr., W.J., Moskowitz, L., 1964. A proposed spectral form for fully developed wind seas based on the similarity theory of S. A. Kitaigorodskii. *Journal of Geophysical Research* 69 (24), 5181–5190.

Provis, D.G., Steedman, R.K., 1985. Wave measurements in the Great Australian Bight. In: *Paper Presented at Australian Conference on Coastal and Ocean Engineering*, IEAust, Christchurch, New Zealand, pp. 51–60.

Reid, J.S., Fandry, C.B., 1994. Wave climate measurements in the Southern Ocean. CSIRO Marine Laboratories Report 223, Hobart, Australia, 105pp.

Simmonds, I., Keay, K., 2000a. Mean Southern Hemisphere extratropical cyclone behaviour in the 40-year NCEP–NCAR reanalysis. *Journal of Climate* 13, 873–885.

Simmonds, I., Keay, K., 2000b. Variability of Southern Hemisphere extratropical cyclone behavior 1958–97. *Journal of Climate* 13, 550–561.

Simmonds, I., Murray, R.J., Leighton, R.M., 1999. A refinement of cyclone tracking methods with data from FROST. *Australian Meteorological Magazine*, Special Edition, pp. 35–49.

- Simmonds, I., Keay, K., Lim, E.-P., 2003. Synoptic activity in the seas around Antarctica. *Monthly Weather Review* 131, 272–288.
- Sterl, A., Caires, S., 2005. Climatology, variability and extrema of ocean waves—the web-based KNMI/ERA-40 Wave Atlas. *International Journal of Climatology* 25 (7), 963–997.
- Tolman, H.L., 2002. User manual and system documentation of WAVEWATCH-III version 2.22. Technical Note 222, NOAA/NWS/NCEP/OMB, 133pp.
- Tolman, H.L., Balasubramanian, B., Burroughs, L.D., Chalikov, D.V., Chao, Y.Y., Chen, H.S., Gerald, V.M., 2002. Development and implementation of wind-generated ocean surface wave models at NCEP. *Weather and Forecasting* 17, 311–333.
- Wood, J.D., Terray, E., Strong, B., Singh, B., 2005. Measurement of deepwater ocean waves from a subsurface mooring. In: *Proceedings of the Oceans 2005—Europe*, vol. 1, pp. 166–171 (doi:10.1109/OCEANSE.2005.1511703).
- Yarnal, B., 1993. *Synoptic Climatology in Environmental Analysis: A Primer*. Belhaven Press, London and Florida, 195pp.
- Young, I.R., 1999. Seasonal variability of the global ocean wind and wave climate. *International Journal of Climatology* 19, 931–950.